Available online at www.sciencedirect.com
ScienceDirect
Journal of the European Ceramic Society 27 (2007) 4461–4471
www.elsevier.com/locate/jeurceramsoc

Synthesis, densification and electrical properties of strontium cerate ceramics

Paul Inge Dahl[a,1], Reidar Haugsrud[b], Hilde Lea Lein[a], Tor Grande[a], Truls Norby[b], Mari-Ann Einarsrud[a,*]

[a] *Department of Materials Science and Engineering, Norwegian University of Science and Technology, NTNU, NO-7491 Trondheim, Norway*
[b] *Centre for Materials Science and Nanotechnology, Department of Chemistry, University of Oslo, NO-0349 Oslo, Norway*

Received 5 January 2007; received in revised form 20 March 2007; accepted 25 March 2007

Abstract

Powders of pure and 5% ytterbium substituted strontium cerate ($SrCeO_3$/$SrCe_{0.95}Yb_{0.05}O_{3-\delta}$) were prepared by spray pyrolysis of nitrate salt solutions. The powders were single phase after calcination in nitrogen atmosphere at 1100 °C ($SrCeO_3$) and 1200 °C ($SrCe_{0.95}Yb_{0.05}O_{3-\delta}$). Dense $SrCeO_3$ and $SrCe_{0.95}Yb_{0.05}O_{3-\delta}$ materials were obtained by sintering at 1350–1400 °C in air. Heat treatment at 850 and 1000 °C, respectively, was necessary prior to sintering to obtain high density. The dense materials had homogenous microstructures with grain size in the range 6–10 μm for $SrCeO_3$ and 1–2 μm for $SrCe_{0.95}Yb_{0.05}O_{3-\delta}$. The electrical conductivity of $SrCe_{0.95}Yb_{0.05}O_{3-\delta}$ was in good agreement with reported data, showing mixed ionic–electronic conduction. The ionic contribution was dominated by protons below 1000 °C and the proton conductivity reached a maximum of ~0.005 S/cm above 900 °C. In oxidizing atmosphere the p-type electronic conduction was dominating above ~700 °C, while the contribution from n-type electronic conduction only was significant above ~1000 °C in reducing atmosphere.

Keywords: $SrCeO_3$; Sintering; Electrical conductivity

---

1. Introduction

Perovskite-type oxide materials (ABO_3), such as orthorhombic strontium cerate, $SrCeO_3$, have been widely studied due to the electrical properties. When properly substituted with rare earth oxides on the cerium site, $SrCeO_3$, exhibit high proton conductivity as first demonstrated by Iwahara et al.[1] This property makes $SrCeO_3$-based ceramics suitable for electrolyte materials in solid oxide fuel cells (SOFCs), hydrogen pumps and sensors.[2–4] In particular $SrCeO_3$ substituted with 5% Yb ($SrCe_{2.95}Yb_{0.05}O_{3-\delta}$) has been classified as one of the perovskite-type oxides with the highest proton conductivity (~0.004 S/cm at 900 °C).[5] However, $SrCeO_3$ based materials have often been rejected for use in commercial devices due to poor mechanical properties and chemical stability.[2]

High stability of strontium carbonate ($SrCO_3$) makes preparation of single phase $SrCeO_3$ powders and bulk materials challenging. $SrCeO_3$ reacts with CO_2 according to Eq. (1) forming $SrCO_3$ which may decompose to strontium oxide (SrO) as described by Eq. (2).[6,7]

$$SrCeO_3(s) + CO_2(g) = SrCO_3(s) + CeO_2(s) \qquad (1)$$

$$SrCO_3(s) = SrO(s) + CO_2(g) \qquad (2)$$

The onset temperature for synthesis of $SrCeO_3$ from a mixture of $SrCO_3$ and CeO_2 (according to Eq. (1)) has been reported to 800 °C and between 1168 and 1190 °C, for reaction in N_2 and CO_2 atmosphere, respectively. The corresponding onset temperature for decomposition of $SrCO_3$ (according to Eq. (2)) in N_2 and CO_2 atmosphere have been reported to 845 °C and between 1220 and 1275 °C, respectively.[6,8] Hence, at lower temperatures (<800 °C), carbonate formation may be critical with respect to phase purity and mechanical properties of $SrCeO_3$ materials. Reactions equivalent to Eqs. (1) and (2) with water should also be considered when operating in atmospheres with high $p(H_2O)$.[7]

---

[*] Corresponding author.
E-mail address: Mari-Ann.Einarsrud@material.ntnu.no (M.-A. Einarsrud).
[1] Present address: SINTEF Materials and Chemistry, NO-0314 Oslo, Norway.

0955-2219/$ – see front matter © 2007 Elsevier Ltd. All rights reserved.
doi:10.1016/j.jeurceramsoc.2007.03.025

Preparation of $SrCeO_3$ powders have been reported by methods such as complexation with EDTA[9] or citric acid[10] and combustion methods,[11] but the dominating synthesis route for these materials is by the solid state ceramic method.[1,6,8,12–20] The main objectives of work on $SrCeO_3$ ceramics have been to investigate the proton conductivity. Hence, densification and microstructure of sintered specimens have not been much in focus. Generally sintering temperatures in the range 1500–1650 °C (in air) have been necessary for preparation of dense (>95%) $SrCeO_3$ and $SrCe_{2.95}Yb_{0.05}O_{3-\delta}$ materials by the solid state ceramic method.[13,15,16,20] Higher densities (>97%) have been obtained from commercial powders by sintering at 1450 °C for 2 h in air,[21] and from powder prepared by a complexation route by sintering at 1300 °C for 12 h in nitrogen atmosphere.[9]

In this investigation we present a complete ceramic processing route to dense $SrCeO_3$ materials with homogenous microstructures, including the synthesis of $SrCeO_3$ powders by spray pyrolysis. The limited literature data on the synthesis and fabrication of $SrCeO_3$ based materials have been the main motivation for the work. Both pure and 5% Yb-substituted $SrCeO_3$ powders have been prepared and the influence of carbonates (and other secondary phases) on the sintering process is particularly addressed. Moreover, characterization of the electrical conductivity has been carried out and the electrical conductivity is described by models based on point defect chemistry.

2. Experimental

2.1. Powder synthesis and sample preparation

Powders of $SrCeO_3$ and $SrCe_{0.95}Yb_{0.05}O_{3-\delta}$ (denoted SC and SC5Yb in the following) were synthesized by spray pyrolysis of nitrate salt solutions. Aqueous solutions of cerium nitrate ($Ce(NO_3)_2 \cdot xH_2O$, Alfa Aesar, 99.5%) and ytterbium nitrate ($Yb(NO_3)_3 \cdot 5H_2O$, Aldrich, 99.9%) were thermogravimetrically standardized and mixed in stoichiometric proportions with dried (250 °C, 24 h) strontium nitrate ($Sr(NO_3)_2$, Merck, >99%), giving a total cation concentration of 0.9 M. The mixed solutions were atomized into a furnace at a rate of 1 L/h. The temperature by the nozzle was 840–845 °C and the output temperature was 540–550 °C. The as-synthesized SC and SC5Yb powders were calcined at 900 °C for 48 h in ambient air. Additional calcination at 1000–1200 °C for 6 h in nitrogen flow ($p_{O_2} < 10^{-4}$ atm, $p_{CO_2} < 2 \times 10^{-7}$ atm) was done in order to remove carbonates and obtain phase pure powders. The calcined powders were ball milled with yttria stabilized zirconia (YSZ) balls in iso-propanol for 6–24 h (ball milling in water resulted in decomposition of the powder). The milled powders were dried at 400 °C for 12 h in ambient air and sieved (150 μm).

Green bodies were made by uniaxial pressing at 64 MPa. Generally powders calcined at higher temperatures (>1000 °C) needed addition of 2 wt% binder (ethyl cellulose, Sigma) in order to increase the green strength and green density to ~55%. No binder was needed for compaction of powders calcined at 900 °C giving green density of 50–53%. Green bodies were sintered in ambient air at temperatures varying from 1250 to 1450 °C in a muffle furnace (SF-4/17, Entech, Sweden). In order to remove carbonate species from the specimens prior to sintering, heat treatment at 850 °C for 24 h and 1000 °C for 1 h was used for sintering of SC and SC5Yb, respectively.

2.2. Characterization of sintered materials

The prepared powders were analyzed and crystal structure confirmed by X-ray diffraction (XRD) (Cu Kα, Philips PW1730/10). Powders from crushed samples sintered at 1400 °C and added 30 wt% Si standard were used to obtain XRD data from which the lattice parameters and theoretical densities were calculated by the Rietveld method. Infrared spectroscopy (IR) was performed on potassium bromide (Merck, KBr for IR spectroscopy Uvasol®) discs containing 1 wt% powder using a Bruker IFS 66v spectrophotometer. Thermogravimetric analysis (TGA) (Netzsch STA 449C Jupiter) on powders was carried out in air with a heating rate of 3 °C/min to 1450 °C. Nitrogen adsorption on de-gassed powders (24 h, 250 °C) was measured (Micromeritics ASAP 2000) using the five point BET equation to obtain specific surface area, from which the particle size was calculated assuming spherical particles.

Dilatometry (Netzch, DIL 402C) on green body cylinders was performed in air with a heating rate of 3 °C/min up to 1450 °C. Density of sintered specimens was measured by the Archimedean method (ISO 5017) in iso-propanol. The prepared powders as well as sintered specimens were studied by scanning electron microscopy (SEM) (Hitachi S-3500N). Average grain size was estimated by the linear intercept method over a minimum of 50 grains.

2.3. Conductivity measurements

A circular Pt electrode (~10 mm diameter) was attached to each side of the SC5Yb specimens, before mounting on top of the support tube in a ProboStat measurement cell for electrochemical characterization (two-electrode measurements).[22] When the purpose was to measure the open-circuit voltage (OCV) from gradients in the pressures of oxygen, hydrogen and water vapor, a gold gasket was placed between the alumina support tube and the specimen. Consequently, the specimen served as a membrane between the inner and the outer gas compartment in the cell. Electrode leads (current supplies and voltage probes) from the cell base were contacted to the electrodes on the specimen. Relatively strong spring loads with alumina parts in the hot zone held the assembly together; to maintain contact between the Pt leads and the electrodes and to facilitate the gold sealing.

The total conductivity was measured in the temperature range 300–1050 °C by means of impedance spectroscopy and at a constant frequency of 10 kHz (Solartron 1260 FRA, oscillation voltages between 0.1 and 1 V) as a function of the oxygen partial pressure; in wet (0.025 atm H_2O) O_2–Ar mixtures for oxidizing and wet (0.025 atm H_2O) H_2–Ar mixtures for reducing conditions, as well as a function of the water vapor partial pressure. The partial conductivities, measured under wet conditions, were calculated based on transport numbers from EMF measurements (Solartron 7150+ high impedance voltmeter) as a function of

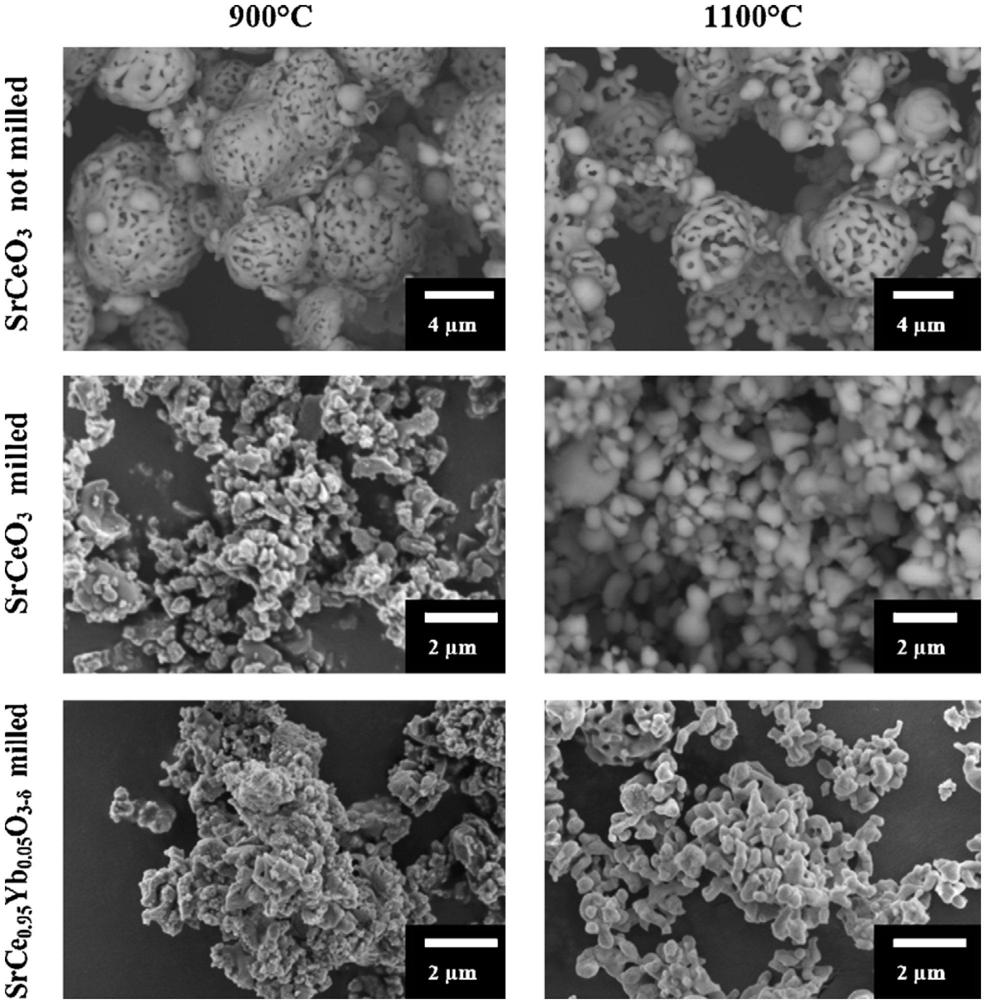

Fig. 1. SEM micrographs of not milled $SrCeO_3$ and $SrCe_{0.95}Yb_{0.05}O_{3-\delta}$ powders calcined at 900 and 1100 °C before and after milling in iso-propanol.

temperature. Details regarding the EMF-method and the set-up of the gas mixer are described in the literature.[23,24]

Impedance spectroscopy in the frequency range 1 MHz–0.1 Hz was applied to determine the different contributions of bulk (b), grain boundaries (gb) and electrodes (e) to the overall impedance. Different circuits were assigned to fit the impedance data depending on the conditions (T, $p(O_2)$ and $p(H_2O)$). Up to 650 °C, it was possible to separate the impedance of bulk and grain boundaries by fitting the impedance data to circuits of parallel resistors (R) and constant phase capacitive elements (Q) in series: $(R_bQ_b)(R_{gb}Q_{gb})(R_eQ_e)$ at temperatures below 450 °C, and $R_b(R_{gb}Q_{gb})(R_eQ_e)$ from 450 to 650 °C. Above 650 °C the bulk and grain boundary impedance could not be separated and the volume resistance, $R_{vol} = R_b + R_{gb}$, was determined. Under conditions where electronic conduction plays a significant role, it has been assumed that $R_{electronic}$, representing the electronic conductance, connects effectively directly between electrodes, yielding circuits which in a simplified version may look like $R_{electronic}R_{vol}(R_eQ_e)$. At temperatures >500 °C the impedance spectra were corrected for a parasitic inductive element, but this is here used only to improve the fit to the other parameters, and is thus not discussed any further. The (R_eQ_e)-elements represent complex processes at the electrodes and can be further separated into several different circuit elements.

3. Results

3.1. Characterization of powders

The morphology of prepared powders is presented by SEM micrographs in Fig. 1. During spray pyrolysis characteristic agglomerates in the form of hollow spheres were formed as seen for the SC powder calcined at 900 °C. The spherical shape was maintained upon heating to 1100 °C, however, some coarsening of the powder was observed. The agglomerates in the SC and SC5Yb powders calcined at 900 °C were effectively broken down to smaller particles by ball milling in iso-propanol. Due to coarsening of the powders during heat treatment at 1100 °C, the particle size after milling seemed somewhat larger in the powders calcined at 1100 °C.

Surface area and calculated particle size for a selection of powders is presented in Table 1. Ball milling of $SrCeO_3$ powder calcined at 900 °C resulted in an increase in surface area, from 1.7 to 5.4 m^2/g. Calcination at 1100 °C gave a slight reduction in surface area to 3.9 m^2/g (after ball milling). The surface area

Table 1
Surface area (SA) of milled $SrCeO_3$ and $SrCe_{0.95}Yb_{0.05}O_{3-\delta}$ powders. Spherical particles were assumed for calculation of the particle size (*D*)

Compound	Calcination temperature (°C)	Calcination time (h)	SA (m^2/g)	*D* (μm)
$SrCeO_3$—not milled	900	48	1.7	0.62
$SrCeO_3$	900	48	5.4	0.19
$SrCeO_3$	1100	6	3.9	0.27
$SrCe_{0.95}Yb_{0.05}O_{3-\delta}$	900	48	17.8	0.06
$SrCe_{0.95}Yb_{0.05}O_{3-\delta}$	1100	6	9.2	0.11

of ball milled SC5Yb powder calcined at 900 °C was 17.8 m^2/g, corresponding to particles 3–8 times smaller compared to that found for the SC powders.

The orthorhombic crystal structure was confirmed for both SC and SC5Yb, and their lattice cell parameters were in good accord with literature.[25,9] X-ray diffractograms of SC and SC5Yb powders are shown in Fig. 2(a) and (b), respectively. Secondary phases (Sr_2CeO_4 and CeO_2) were present in the SC powder after calcination at 900 °C. After calcination at 1000 °C in nitrogen flow these phases were still detected by XRD, however, calcination at 1100 °C resulted in phase pure SC powder. Larger amounts of secondary phases were detected in the SC5Yb powder calcined at 900 °C in air. In addition to the secondary phases found in the SC powders, $SrCO_3$ was detected in SC5Yb powder calcined at 900 °C. $SrCO_3$ was not detected in the SC5Yb powder calcined at 1000 °C in nitrogen flow, but both Sr_2CeO_4 and CeO_2 were present. Traces of Sr_2CeO_4 were also detected after calcination at 1100 °C but the powder was apparently phase pure after calcination at 1200 °C. The sintered materials were phase pure according to XRD, and XRD on the surface of sintered specimen exposed to ambient atmosphere for 2 weeks gave no indications of formation of $SrCO_3$.

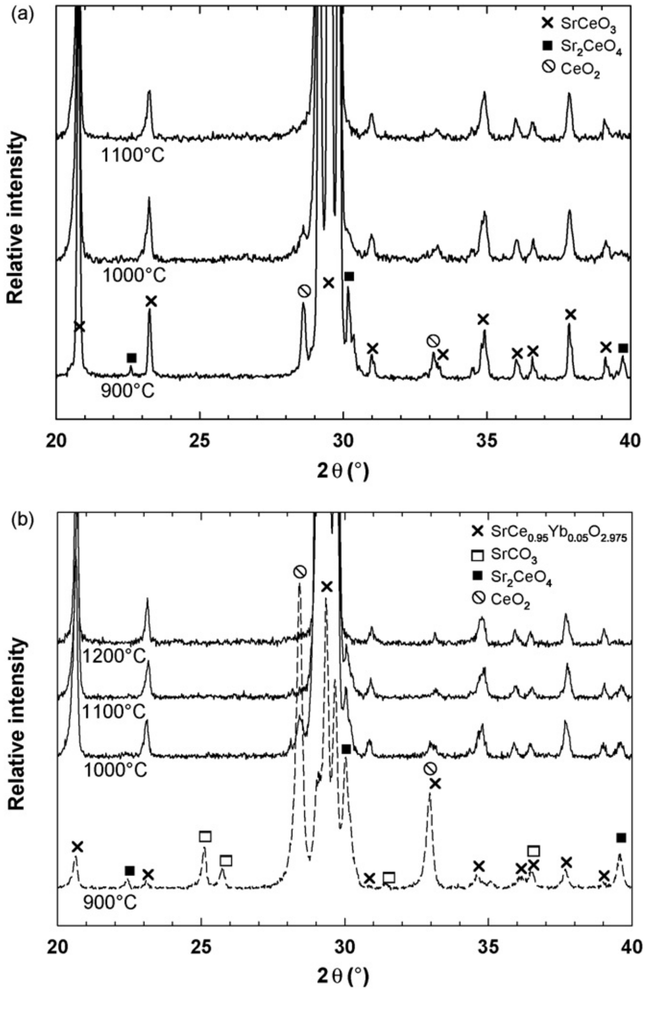

Fig. 2. X-ray diffractograms of (a) $SrCeO_3$ powders and (b) $SrCe_{0.95}Yb_{0.05}O_{3-\delta}$ powders calcined in ambient air at 900 °C and in nitrogen flow from 1000 to 1200 °C.

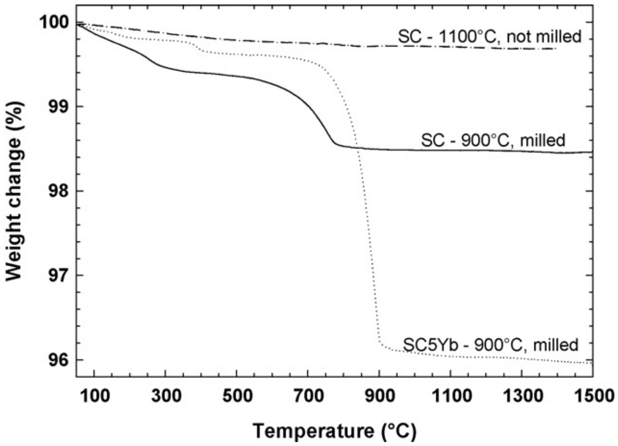

Fig. 3. TG curves obtained from milled $SrCeO_3$ (SC) and $SrCe_{0.95}Yb_{0.05}O_{3-\delta}$ (SC5Yb) powders calcined at 900 °C as well as SC powder calcined at 1100 °C before milling.

Fig. 3 shows TG data for SC and SC5Yb powders. Significant weight loss was observed for both SC and SC5Yb powder calcined at 900 °C and ball milled in iso-propanol. The observed weight loss below 400 °C (mainly seen for SC powder calcined at 900 °C) is most likely due to adsorption of $CO_2$and/or water from the atmosphere as all powders were dried at 400 °C after milling. As seen from Fig. 3, the main weight loss of milled powders was found between 700 and 800 °C for SC and around 900 °C for SC5Yb. This weight loss is associated with decomposition of $SrCO_3$. The higher loss (4.0%) for SC5Yb compared to SC (1.6%) is in agreement with the XRD data. A total weight loss of ∼0.3% was observed for SC powder calcined at 1100 °C. A low content of $SrCO_3$ after calcination at 1100 °C is inferred based on the thermogravimetry.

IR spectra of SC/SC5Yb powders calcined at different temperatures are presented in Fig. 4. A reference spectrum of $SrCO_3$ is also included. The broad band in the range of 500 to 800 cm^{-1}, observed for all powders, is due to the stretching of the metal–oxygen bonds.[26] The characteristic frequencies for $SrCO_3$ are also found in the spectra of SC and SC5Yb powders calcined at 900 °C, respectively. Higher intensity of the carbonate bands, indicate larger amount of $SrCO_3$ in the SC5Yb powder compared to SC. SC powders calcined at 1000 and 1100 °C were carbonate free according to the IR spectra. SC5Yb powders calcined at higher temperatures (1000–1100 °C) show similar behaviour as observed for SC. IR spectra of ball milled powders

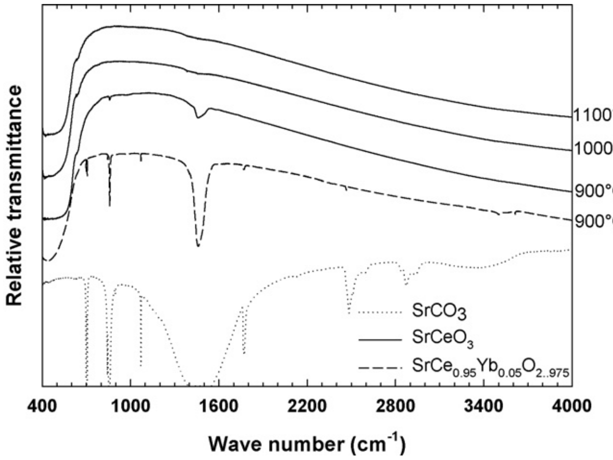

Fig. 4. IR spectra of $SrCO_3$ powder, $SrCe_{0.95}Yb_{0.05}O_{3-\delta}$ and $SrCeO_3$ powders calcined 900 °C in air as well as $SrCeO_3$ powders calcined at 1000 °C and 1100 °C in nitrogen atmosphere.

indicated that $SrCO_3$ was reintroduced by CO_2 adsorption from the air or from reaction with residual iso-propanol in the powder. A minor peak near 3500 cm^{-1} evidenced the presence of OH in SC5Yb calcined at 900 °C, while in undoped $SrCeO_3$ this peak is absent in line with expectations.

3.2. Densification

The linear shrinkage versus temperature presented in Fig. 5(a) shows an onset for densification at ∼800 °C for SC and ∼1000 °C for SC5Yb, both calcined at 900 °C. The presintering feature above 900 °C for SC5Yb is most likely due to decomposition of residual $SrCO_3$, resulting in evolution of CO_2 gas that could cause expansion of closed pores in the material. Calcination at 1100 °C resulted in a small shift in the onset temperature for densification. Though the onset temperature for densification is lower for SC, the sintering rate for this compound is lower than for SC5Yb, as displayed in Fig. 5(b). The highest sintering rate (Fig. 5(b)) for SC calcined at 900 °C was found at ∼1150 °C and as high as ∼1375 °C for SC calcined at 1100 °C. In comparison the highest sintering rate for SC5Yb calcined at 900 and 1100 °C was ∼1330 and ∼1370 °C, respectively.

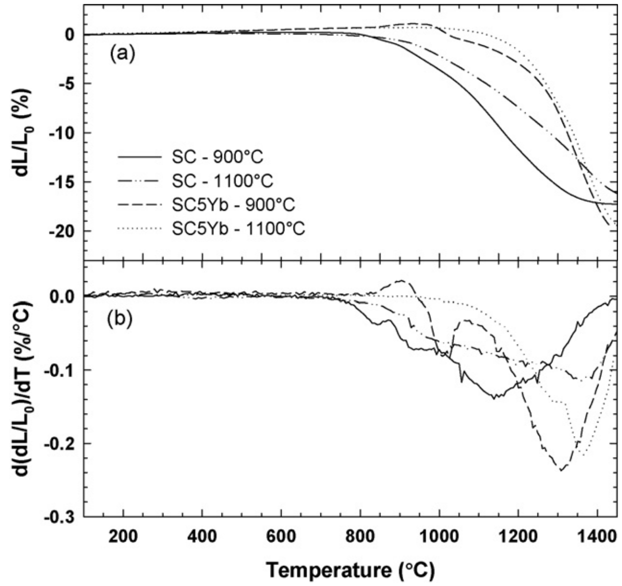

Fig. 5. (a) Linear shrinkage and (b) sintering rate from associated derivative curves for $SrCeO_3$ (SC) and $SrCe_{0.95}Yb_{0.05}O_{3-\delta}$ (SC5Yb) after calcination at 900 °C and 1100 °C.

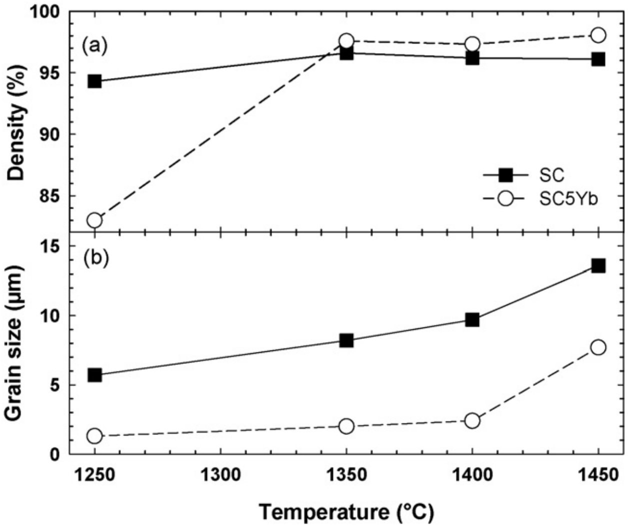

Fig. 6. (a) Density and (b) estimated grain size of $SrCeO_3$ (SC) and $SrCe_{0.95}Yb_{0.05}O_{3-\delta}$ (SC5Yb) specimens sintered at indicated temperatures for 2 h in ambient air.

Fig. 6 displays the variation in density and estimated grain size as a function of temperature during isothermal sintering of SC and SC5Yb. The presintering heat treatment at 850 °C for 24 h for SC and 1000 °C for 1 h for SC5Yb resulted in 1–4% reduction of closed porosity. As seen in Fig. 6(a), the density of SC and SC5Yb increases when the temperature is increased from 1250 to 1350 °C, however further increase in temperature gave little change in density. After sintering at 1350 °C, the density was 96.6 and 97.6% of theoretical density for SC and SC5Yb, respectively.

3.3. Microstructure and grain growth

Estimated grain size in sintered SC and SC5Yb specimens are presented in Fig. 6(b). The grain size in SC increased from ∼6 to ∼14 µm when the sintering temperature was increased from 1250 to 1450 °C. For SC5Yb the grain growth was less severe giving average grain size in the range of 1 to 2 µm after sintering at 1250–1400 °C. Sintering at 1450 °C, however, resulted in grain size of ∼8 µm for this composition as well. The homogenous microstructures of sintered SC and SC5Yb specimens are displayed by SEM micrographs in Fig. 7. While the grain size of the SC specimens were rather large, even after sintering at 1250 °C, SC5Yb specimen exhibits grains of ∼1 µm, however this specimen appears not fully dense. The inevitable amount of closed porosity observed in SC specimens, due to higher mobility of grain boundaries compared to pores, was not observed in the SC5Yb specimens sintered at temperatures up to 1400 °C. Sintering at 1450 °C produced larger grains resulting in some

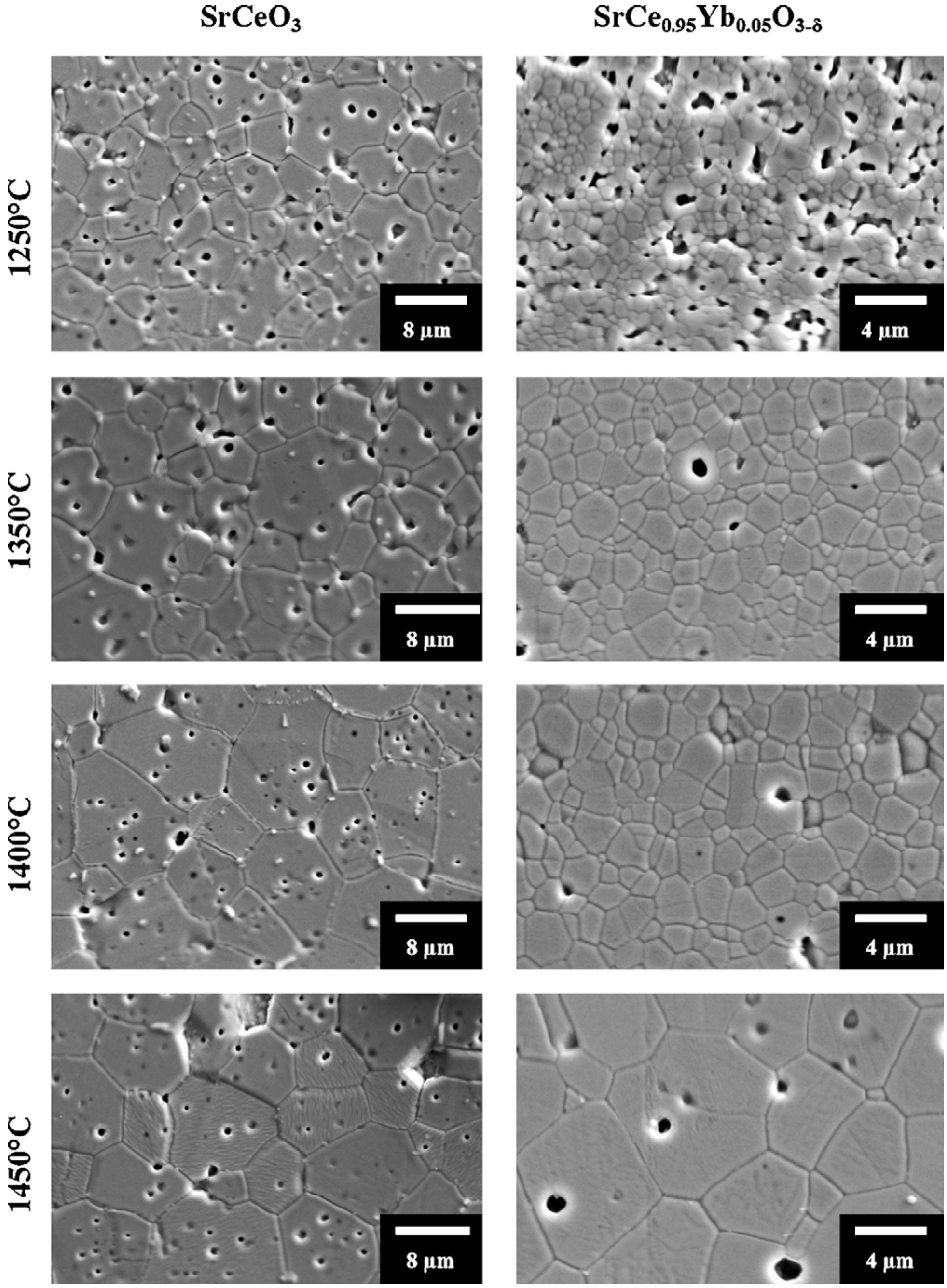

Fig. 7. SEM micrographs of polished and etched (1200 °C, 12 min) surfaces of $SrCeO_3$ and $SrCe_{0.95}Yb_{0.05}O_{3-\delta}$ specimens sintered for 2 h at 1250 °C–1450 °C.

enclosed pores for SC5Yb as well. The severe grain growth in SC resulted in microcracking due to the anisotropic crystal structure of the orthorhombic $SrCeO_3$ reducing the mechanical properties of this material. Finally, BS images and EDS gave no evidence of segregation of Yb along grain boundaries or contamination of the samples during firing.

3.4. Electrical properties

Conductivities as a function of the inverse temperature for SC5Yb (sintered at 1350 °C and 2 h) in wet oxygen (0.025 atm H_2O + 0.975 atm O_2) and wet hydrogen (0.025 atm H_2O + 0.975 atm H_2) are presented in Fig. 8(a) and (b), respectively. These figures include the total AC (10 kHz) conductivity measured in continuous temperature ramps (12 °C/h), along with partial conductivities deconvoluted from impedance spectroscopy at selected temperatures in wet hydrogen (Fig. 8(b)). The proton and oxygen ion conductivities are similar under oxidizing and reducing conditions, whereas the electronic contribution under oxidizing conditions (p-type) is higher than under reducing conditions (n-type). One should note that the OCV of concentration cells has only been measured in the temperature region where the proton transport number is less than 1 and below the melting point of gold (700–1050 °C). The total

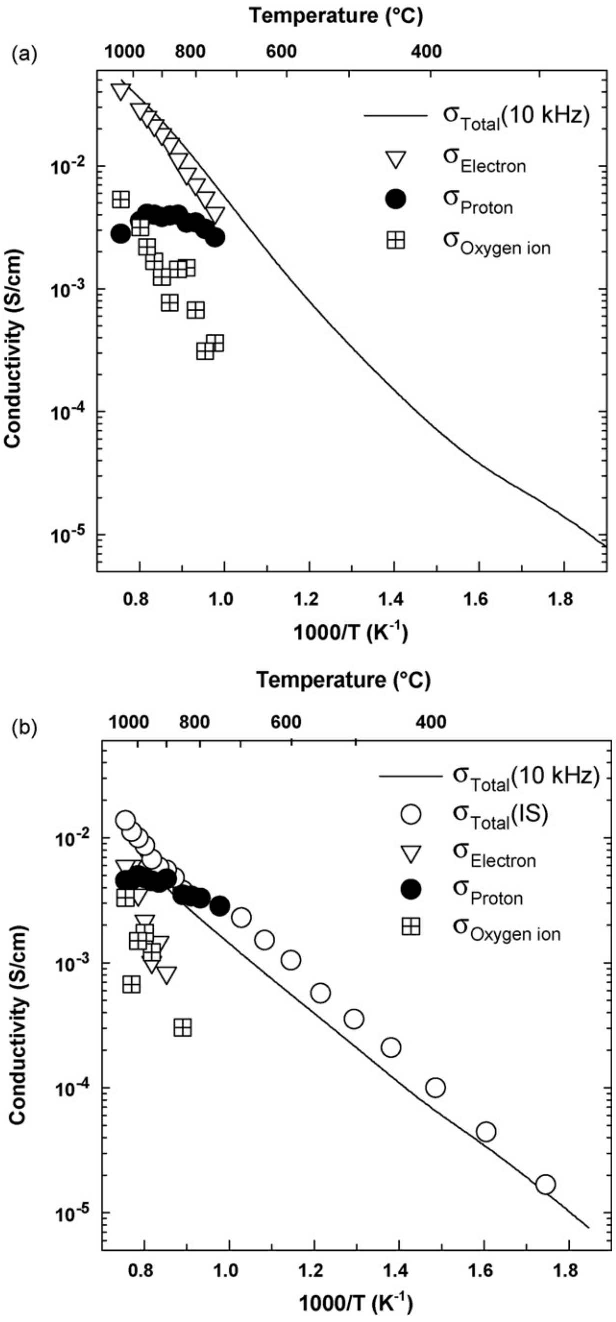

Fig. 8. Total conductivity and partial conductivities as a function of the inverse absolute temperature for $SrCe_{0.95}Yb_{0.05}O_{3-\delta}$ in (a) wet oxygen and (b) wet hydrogen. σ_{Total}(10 kHz) and σ_{Total}(IS) are obtained from a continuous ramp at 10 kHz and impedance spectroscopy with 50 °C steps, respectively. The sample was sintered for 2 h at 1350 °C.

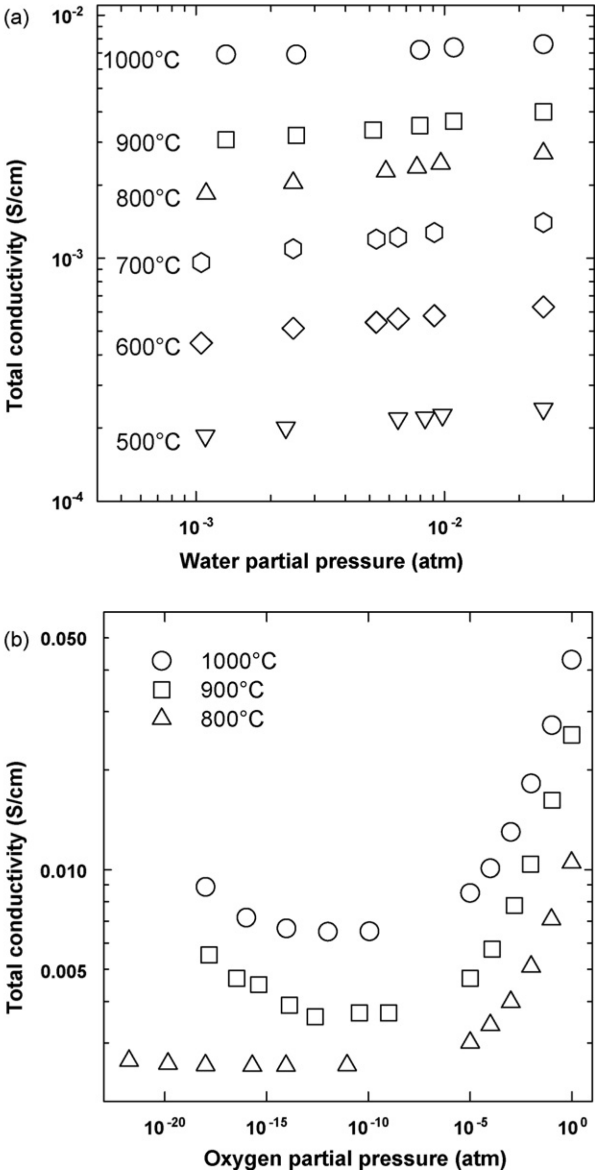

Fig. 9. Total conductivity of $SrCe_{0.95}Yb_{0.05}O_{3-\delta}$ specimens with (a) varying water vapor partial pressure, measured in $H_2 + H_2O + Ar$ mixtures with constant p_{H_2}/p_{H_2O} ratio of 0.025/0.975 at 500–1000 °C, and (b) varying oxygen partial pressure at constant $p_{H_2O} = 0.025$ atm in the range of 800–1000 °C. The sample was sintered for 2 h at 1350 °C.

conductivities measured at temperatures lower than ~700 °C are predominantly protonic, although this is not indicated in Fig. 8, since it has not been directly measured. The grain boundary resistance in this material was low and, as mentioned, the bulk and grain boundary impedance could not be separated above 650 °C.

The water vapor partial pressure dependence of the total conductivity from 500 to 1000 °C, as measured in hydrogen, is shown in Fig. 9(a). The total conductivity increases as a function of increasing water vapor partial pressure. The typical conductivity behavior observed for a mixed ionic–electronic conductor upon large variations in the oxygen partial pressure, is shown in Fig. 9(b), for temperatures in the range 800–1000 °C. The total conductivity increases with decreasing oxygen partial pressures under reducing conditions, and increases with increasing oxygen partial pressures under oxidizing conditions. These two behaviors reflect an increasing n-type and p-type contribution to the total conductivity, respectively. Between these two regimes the total conductivity is essentially independent of the oxygen partial pressure reflecting ionic conduction. Below 800 °C under reducing conditions, the conductivity is predominantly ionic showing no significant n-type electronic conduction. One should note that the total conductivity declines with time, and that this seems to depend particularly on the time measured under wet conditions and at low temperature.

4. Discussion

4.1. Powder characteristics

As demonstrated in this work, phase pure $SrCeO_3$ powders can be prepared by spray pyrolysis followed by calcination at 1100–1200 °C in nitrogen atmosphere. Fine powders with particle size down to ∼60 nm have been obtained by ball milling of calcined powders, however some coarsening was observed with increasing calcination temperature. The TG analysis (Fig. 3) of SC powders in air indicates that $SrCO_3$ introduced during ball milling is removed below 800 °C, in agreement with reported onset temperature for synthesis of SC from a mix of $SrCO_3$ and CeO_2 in nitrogen.[6] The IR spectrum of SC calcined at 900 °C (Fig. 4), however, shows that small amount of $SrCO_3$ is present in the powder even before milling. A larger amount of $SrCO_3$ in the SC5Yb powder calcined at 900 °C, confirmed by XRD (Fig. 2(b)) and IR (Fig. 4) and assisted by the larger weight loss from TG analysis (Fig. 3), indicates a stabilization of this secondary phase by substitution with Yb. The presence of Sr_2CeO_4 and CeO_2 were also more pronounced in case of the SC5Yb powder. Sr_2CeO_4 was detected by XRD in the SC5Yb powder after calcination at 1100 °C, but not in the SC powder after calcination at 1000 °C. These features may be explained by the more basic nature of Yb-substituted material, as reported for ceria,[27] which in turn, e.g. will make the material more susceptible to CO_2.

4.2. Densification and microstructure

By introducing a heat treatment at 850 and 1000 °C prior to sintering, dense SC and SC5Yb materials, with well defined microstructures, were obtained by sintering for 2 h in air at 1350–1400 °C. SC was found to sinter at a lower temperature compared to SC5Yb and onset temperatures for sintering being around ∼200 °C lower. The higher sintering temperature in the Yb-substituted material can not be assigned to any ionic size effects, as the ionic radius of Yb^{3+} equals that of Ce^{4+}.[28] The introduction of oxygen vacancies in the material is also unlikely to increase the sintering temperature. Sintering is rate limited by diffusion of cations (the slowest moving ions), and oxygen vacancies should lower the activation barrier for cation diffusion. The shift in onset temperature for sintering may be explained by the presence of secondary phases, inhibiting the sintering in the SC5Yb material. Sr_2CeO_4 was detected in the SC5Yb powder, even after calcination at 1100 °C. All secondary phases seem to vanish at higher temperatures (1200 °C), however, at such temperatures coarsening of the powder will reduce the sinterability as well. Despite lower onset temperature, the sintering rate was higher in the SC5Yb material compared to SC, as demonstrated in Fig. 5. This effect may be explained by larger surface area in starting powders compared to that of SC. Densities of 96–98% of SC and SC5Yb materials sintered at 1350–1450 °C in air are comparable to reported densities >98% obtained by solid state ceramic method and sintering at 1550–1600 °C in air for 10–12 h,[16,17] and from powders prepared by complexation route, by sintering at 1300 °C for 12 h in nitrogen flow.[9]

Homogenous, fine-grained microstructures were obtained for the SC5Yb specimens sintered up to 1400 °C. The more severe grain growth in the SC materials, with resulting trapped pores indicates a high mobility of grain boundaries compared to pores. The reduced growth in SC5Yb may, as the sinterability, be explained by the presence of secondary phases in the material. At elevated sintering temperatures the secondary phases will disappear (presuming stoichiometric cation ratio in the starting powder), alleviating the grain boundary pinning. This may be the effect observed in SC5Yb when increasing the sintering temperature from 1400 to 1450 °C, resulting in remarkable grain growth.

Due to the anisotropic crystal structure of $SrCeO_3$, microcracking was observed in large grained SC materials (>6 μm), while the finer grained (1–2 μm) SC5Yb materials were resistant towards microcracking. Based on these observations the critical grain size may be estimated between 2 and 6 μm. In a comparable work, grain size of ∼7 μm has been reported for dense SC5Yb materials,[9] however studies of microstructure and grain size in these materials are rare. The commonly used solid-state ceramic route produces coarse powders, hence, high sintering temperatures (>1500 °C) are needed to obtain dense materials. Consequently, the sintered materials will consist of rather large grains (10–20 μm).[13] This exceeds the suggested critical size for microcracking, which in turn may explain the poor mechanical properties observed for $SrCeO_3$ materials.[7] Our suggestion is supported by the high mechanical bending strength reported for SC5Yb with grain size of 7 μm.[9] Observations made in the present work, points out the importance of high quality starting powders and controlled densification, with respect to the mechanical properties of the sintered $SrCeO_3$-based materials.

4.3. Conductivity

The conductivity results generally reflect the behaviour reported in the literature on acceptor substituted $SrCeO_3$.[1,2,5,12–18,29–34] $SrCe_{0.95}Yb_{0.05}O_{3-\delta}$ exhibit mixed ionic–electronic conduction where the ionic contribution is predominated by protons below ∼1000 °C. The proton conductivity reaches a maximum of ∼0.005 S/cm above 900 °C (in wet atmosphere). Oxygen ion conductivity becomes the major ionic charge carrier above 1000 °C. The p-type conductivity is considerably higher under oxidizing conditions than the corresponding n-type conductivity under reducing conditions. This conductivity behavior can be interpreted with basis in a few elementary point defect reactions. Substitution of trivalent Yb for tetravalent Ce yields an effectively negative defect (acceptor) that must be charge-compensated either by consumption of other effectively negative or formation of effectively positive defects. In $SrCeO_3$ charge-compensation occurs by formation of oxygen vacancies according to Eq. (3):

$$Yb_2O_3 + 2SrO = 2Yb'_{Ce} + 2Sr^{x}_{Sr} + v_{O}^{\bullet\bullet} + 5O^{x}_{O} \qquad (3)$$

Under wet conditions oxygen vacancies may be hydrated through interaction with water vapor. The protonic defect that forms is assumed to be associated with a structural oxygen ion through Eq. (4):

$$H_2O(g) + v_O^{\bullet\bullet} + O_O^x = 2OH_O^{\bullet} \qquad (4)$$

Native defects are furthermore in equilibrium with the surrounding atmosphere, as shown in Eq. (5) for oxygen vacancies in equilibrium with electron holes:

$$O_O^x + 2h^{\bullet} = v_O^{\bullet\bullet} + \tfrac{1}{2}O_2(g) \qquad (5)$$

By taking the intrinsic ionization between electron holes and electrons into account all the point defects necessary to model the behavior encountered during this investigation are in place. However, in order to obtain a full mathematical description of the defect structure, and to determine physicochemical parameters reflecting the conductivity characteristics, the site balance and the electroneutrality must be included.[35] Within the experimental window of the present investigation, acceptor doping in $SrCeO_3$ has, generally, been concluded to be charge compensated predominantly by oxygen vacancies and protons. Hence, the electroneutrality condition may be expressed by Eq. (6):

$$[Yb'_{Ce}] = 2[v_O^{\bullet\bullet}] + [OH_O^{\bullet}] \qquad (6)$$

By combining this electroneutrality and the site balance with Eq. (4), the concentration of protons and oxygen vacancies may be resolved. Moreover, the conductivity of the different charge carriers (indexed i) is proportional to their concentration (c_i) and mobility (μ_i), $\sigma_i = z_i e c_i \mu_i$. On these bases the dependencies of the partial and total conductivities with variations in the conditions can be modelled. Thermodynamic parameters extracted from this modelling include the standard entropy and enthalpy of the hydration reaction in Eq. (4), $\Delta S^\circ = -125 \pm 5$ J/molK, $\Delta H^\circ = -145 \pm 10$ kJ/mol and, moreover, the preexponential mobility and the activation enthalpy of defect mobility for the protons and oxygen vacancies: $\mu_o(H^+) = 20 \pm 5\ \mathrm{cm^2\ K/Vs}$, $\Delta H_{mob}(H^+) = 55 \pm 5$ kJ/mol, $\mu_o(v_O^{\bullet\bullet}) = 20 \pm 10\ \mathrm{cm^2\ K/Vs}$, $\Delta H_{mob}(v_O^{\bullet\bullet}) = 60 \pm 5$ kJ/mol. Since it is not possible to resolve independent expressions for the concentration of electrons and electron holes, only the activation energies for p- and n-type conductivity can be listed: 65 kJ/mol and 350 kJ/mol for electron holes and electrons respectively at constant partial pressure of O_2 and H_2O. As a first approximation the entropy of the hydration reaction was assumed to be −120 J/mol.

Fig. 10(a) demonstrates, by way of example, the fit of the parameter-set to the water vapor partial pressure dependence in hydrogen. Moreover, Fig. 10(b) illustrates how the different partial conductivities individually influence the overall functional water vapor partial pressure dependence at 500 and 1000 °C. One may note here how protons predominate at the low temperature as a consequence of the exothermic nature (negative enthalpy) of the hydration of oxygen vacancies. Oxygen ion conductivity barely influences the total conductivity even under dry conditions at 500 °C, and n-type electronic conduction is orders of magnitude lower than the ionic conductivity. By increasing the temperature, the influence of protons decreases as indicated by reduced proton concentration relative to the oxygen vacancy concentration. At high temperature, under these rather reducing conditions, also n-type conduction comes into play, particularly at high water vapor partial pressures. The shift in the relative influence of the three charge-carriers within the 500 °C temperature interval explains the observed change in curvature of the functional water vapor partial pressure dependence (Fig. 10(a) and (b)).

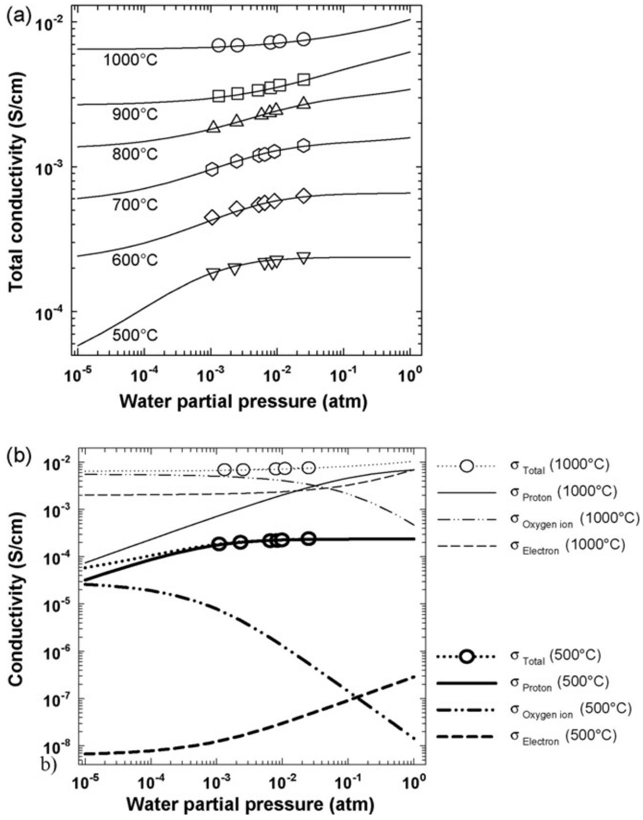

Fig. 10. (a) Total conductivity curves fit to the experimental data for $SrCe_{0.95}Yb_{0.05}O_{3-\delta}$, for varying water vapor partial pressure, in hydrogen from 500 to 1000 °C. (b) Total and partial conductivities with varying partial pressure of water vapor at 500 °C (bold curves) and 1000 °C (slim curves). Circles and lines experimental results data and modeled conductivity curves, respectively. The sample was sintered for 2 h at 1350 °C.

Despite the extensive literature on the functional properties of the acceptor substituted $SrCeO_3$, only a few investigations have so far derived a set of physicochemical properties as reported here. The thermodynamics of the dissolution of water according to the reaction in Eq. (4) have been measured by thermogravimetry and also estimated from conductivity measurements.[17,36,37] Hydration enthalpies are reported in the range from −115 to −160 kJ/mol, in agreement with the value of −145 kJ/mol obtained here.

The degradation in the total conductivity encountered during these experiments may have several reasons. The basic high-temperature proton conducting perovskites, in particular $BaCeO_3$ and $SrCeO_3$, are renowned for their reactivity towards CO_2. However, since gas mixtures with relatively low levels of CO_2 have been applied during this investigation, this is not believed to cause the decline observed in the total conductivity with time. More likely this is a result of decomposition of $SrCeO_3$ to $Sr(OH)_2$ and CeO_2,[7] due to long-term exposure in wet atmospheres at relatively low temperature (slow temperature ramps down to 300 °C). We would also like to point out that $SrCeO_3$ may react with Pt, especially under reducing conditions, and that this may change both the properties of the material and affect the quality and extension of the electrodes.

5. Conclusions

Spray pyrolysis has been proven a good method for preparing fine powders of orthorhombic $SrCeO_3$ and $SrCe_{0.95}Yb_{0.05}O_{3-\delta}$. Secondary phases in the as-synthesized powders were removed by calcination in CO_2-free atmosphere at 1100 and 1200 °C, respectively. Dense (>96%) materials with homogenous microstructures have successfully been prepared by sintering at 1350–1400 °C. Due to lower mobility of grain boundaries in the $SrCe_{0.95}Yb_{0.05}O_{3-\delta}$ material, the grain size (1–2 μm) was smaller than for $SrCeO_3$ (>6 μm). We have suggested that grain size below ∼6–7 μm is required to avoid microcracking and poor mechanical properties in $SrCeO_3$-based materials due to their anisotropic crystal structure. The electrical properties of the Yb-substituted materials were in good agreement with literature data, showing p-type conductivity in oxidizing and n-type conductivity in reducing atmosphere. The ionic contribution to the total conductivity is predominately protonic below 1000 °C and the protonic conductivity reaches a maximum of 0.005 S/cm at 1000 °C.

Acknowledgements

Work was supported by the Research Council of Norway, NANOMAT Grant No. 158517/431 (Functional Oxide for Energy Technology). Øystein Andersen; NTNU, is acknowledged for assisting in the production of the powders.

References

1. Iwahara, H., Esaka, T., Uchida, H. and Maeda, N., Proton conduction in sintered oxides and it's application to steam electrolysis for hydrogen production. *Solid State Ionics*, 1981, **3/4**, 359–363.
2. Iwahara, H., Technological challenges in the application of proton conducting ceramics. *Solid State Ionics*, 1995, **77**, 289–298.
3. Norby, T., Solid-state protonic conductors: principles, properties, progress and prospects. *Solid State Ionics*, 1999, **125**, 1–10.
4. Schober, T., Applications of oxidic high-temperature proton conductors. *Solid State Ionics*, 2003, **162/163**, 277–281.
5. Yajima, T. and Iwahara, H., Studies on proton behaviour in doped perovskite-type oxides. II. Dependence of equilibrium hydrogen concentration and mobility on dopant content in Yb-doped $SrCeO_3$. *Solid State Ionics*, 1993, **53–56**, 983–988.
6. Scholten, M. J. and Schoonman, J., Synthesis of strontium and barium cerate and their reaction with carbon dioxide. *Solid State Ionics*, 1993, **61**, 83–91.
7. Kreuer, K.-D., On the development of proton conducting materials for technological applications. *Solid State Ionics*, 1997, **97**, 1–15.
8. Shirsat, A. N., Kaimal, K. N. G., Bharadwaj, S. R. and Das, D., Thermodynamic stability of $SrCeO_3$. *J. Solid State Chem.*, 2004, **177**, 2007–2013.
9. de Vires, K. J., Electrical and mechanical properties of proton conducting $SrCe_{0.95}Yb_{0.05}O_{3-\alpha}$. *Solid State Ionics*, 1997, **100**, 193–200.
10. Cheng, S., Gupta, V. K. and Lin, J. Y. S., Synthesis and hydrogen permeation properties of asymmetric proton-conducting ceramic membranes. *Solid State Ionics*, 2005, **176**, 2653–2662.
11. Chavan, S. V. and Tyagi, A. K., Preparation of $Sr_{0.09}Ce_{0.91}O_{1.91}$, $SrCeO_3$, and Sr_2CeO_4 by glycine-nitrate combustion: crucial role of oxidant-to-fuel ratio. *J. Mater. Res.*, 2004, **19**(11), 3181–3188.
12. Scherban, T. and Nowick, A. S., Bulk protonic conduction in Yb-doped $SrCeO_3$. *Solid State Ionics*, 1989, **35**, 189–194.
13. Matsunami, N., Yajima, T. and Iwahara, H., Permeation of implanted deuterium through $SrCeO_3$ (5% Yb). *Nuclear Instruments and Methods in Physics Research*, 1992, **B65**, 278–281.
14. Kosacki, I., Schoonman, J. and Balanski, M., Raman scattering and ionic transport in $SrCe_{1-x}Yb_xO_3$. *Solid State Ionics*, 1992, **57**, 345–351.
15. Iwahara, H., Yajima, T., Hibino, T., Ozaki, K. and Suzuki, H., Protonic conduction in calcium, strontium and barium zirconates. *Solid State Ionics*, 1993, **61**, 65–69.
16. Kosacki, I. and Tuller, H. L., Mixed conductivity in $SrCe_{0.95}Yb_{0.05}O_3$ protonic conductors. *Solid State Ionics*, 1995, **80**, 223–229.
17. Reichel, U., Arons, R. R. and Schilling, W., Investigation of n-type electronic defects in the protonic conductor $SrCe_{1-x}Y_xO_{3-\alpha}$. *Solid State Ionics*, 1996, **86–88**, 639–645.
18. Matzke, T. and Cappadonia, M., Proton conductive perovskite solid solutions with enhanced mechanical stability. *Solid State Ionics*, 1996, **86–88**, 659–663.
19. Chavan, S. V. and Tyagi, A. K., Sub-solidus phase equilibria in CeO_2–SrO system. *Thermochimica Acta*, 2002, **390**, 79–82.
20. Matsumoto, H., Shimura, T., Iwahara, H., Higuchi, T., Yashiro, K., Kaimai, A. *et al.*, Hydrogen separation using proton-conducting perovskites. *Journal of Alloys and Compounds*, 2006, **408–412**, 456–462.
21. Taherparvar, H., Kilner, J. A., Baker, R. and Sahibzada, M., Effect of humidification at anode and cathode in proton-conducting SOFCs. *Solid State Ionics*, 2003, **162/163**, 297–303.
22. Norby, T., private communication, Norwegian Electro Ceramics AS, Norway.
23. Norby, T., EMF method determination of conductivity contributions from protons and other ions in oxides. *Solid State Ionics*, 1988, **28–30**, 1586–1591.
24. Sutija, D. P., Norby, T. and Björnbom, P., Transport number determination by the concentration-cell/open-circuit voltage method for oxides with mixed electronic, ionic and protonic conductivity. *Solid State Ionics*, 1995, **77**, 167–174.
25. Ranlov, J. and Nielsen, K., Crystal-structure of the high-temperature protonic conductor $SrCeO_3$. *J. Mater. Chem.*, 1994, **4**, 867–868.
26. Nakamoto, K., *Infrared and Raman Spectra of Inorganic and Coordination Compounds* (*2nd ed.*). John Wiley & Sons Inc., New York, 1997.
27. Mokkelbost, T., Kaus, I., Grande, T. and Einarsrud, M.-A., Combustion synthesis and characterization of nanocrystalline CeO_2-based powders. *Chem. Mater.*, 2004, **16**, 5489–5494.
28. Shannon, R. D., Revised effective ionic radii and systematic studies of interatomic distances in halides and chalcogenides. *Acta Cryst. A*, 1976, **32**, 751–767.
29. Uchida, H., Maeda, N. and Iwahara, H., Relation between proton and hole conduction in $SrCeO_3$-based solid electrolytes under water-containing atmospheres at high temperatures. *Solid State Ionics*, 1983, **11**, 117–124.
30. Uchida, H., Yoshikawa, H., Eseka, T., Ohtsu, S. and Iwahara, H., Formation of protons in $SrCeO_3$-based proton conducting oxides. Part II. Evaluation of proton concentration and mobility in Yb-doped $SrCeO_3$. *Solid State Ionics*, 1986, **36**, 89–95.
31. Yajima, T., Iwahara, H., Uchida, H. and Koide, K., Relation between proton conduction and concentration of oxide ion vacancy in $SrCeO_3$ based sintered oxides. *Solid State Ionics*, 1990, **40/41**, 914–917.
32. Hibino, T., Mizutani, K., Yajima, T. and Iwahara, H., Evaluation of proton conductivity in $SrCeO_3$ $BaCeO_3$, $CaZrO_3$ and $SrZrO_3$ by temperature programmed desorption method. *Solid State Ionics*, 1992, **57**, 303–306.

33. Iwahara, H., Proton conducting ceramics and their applications. *Solid State Ionics*, 1996, **86–88**, 9–15.
34. Schober, T., Krug, F. and Schilling, W., Criteria for the application of high temperature proton conductors in SOFCs. *Solid State Ionics*, 1997, **97**, 369–373.
35. Haugsrud, R. and Norby, T., Proton conduction in rare-earth ortho-niobates and ortho-tantalates. *Nature Materials*, 2006, **5**, 193–196.
36. Yajima, T. and Iwahara, H., Studies on behavior and mobility of protons in doped perovskite-type oxides. I. In situ measurement of hydrogen concentration in $SrCe_{0.95}Yb_{0.05}O_{3-\alpha}$ at high temperatures. *Solid State Ionics*, 1992, **50**, 281–286.
37. Krug, F., Schober, T. and Springer, T., In situ measurements of the water uptake in Yb doped $SrCeO_3$. *Solid State Ionics*, 1995, **81**, 111–118.